

Potential discrete element simulation applications ranging from airborne fines to pellet beds

Otis R. Walton
Grainflow Dynamics
walton@grainflow.com

Copyright © 2004 SAE International

ABSTRACT

Under micro-gravity, lack of sedimentation allows all scales of airborne particulates to participate in the formation of clusters and aggregates. As observed in the International Space Station (ISS), the resulting very-low-density dust aggregates can collect on ventilation inlet screens and duct walls. Discrete Element Method (DEM) simulations, utilizing cohesive interparticle forces and bending-moment interactions, are a tool that can assist in understanding the build-up, compaction, and removal of such agglomerate beds. At a different length-scale, high pellet-pellet contact stresses can be developed in the thermally cycled packed granular beds of air revitalization equipment (possibly fracturing pellets and/or producing unwanted fines). The limits and capabilities of DEM models to simulate these and other particulate systems is discussed.

INTRODUCTION

AIRBORNE FINE PARTICULATES – Under micro-gravity, sedimentation and thermal convection forces do not contribute to airborne particulate motion. Thus, interparticle cohesion, forced convection, and Brownian diffusion become much more important than they are for comparable-sized particles in a terrestrial environment. Particulates generated in crew habitat areas are comprised of the expected constituents (*i.e.*, skin flakes, fibers from hair, clothing, and paper, as well as other organic and inorganic particles); however, larger particles do not settle out like they would terrestrially. The longer airborne lifetimes mean that larger particles participate in cluster and aggregate formation to a greater degree than they would on earth. In long duration space missions most dust aggregates will eventually enter the ventilation system, and many will deposit through a process of ‘envelope’ impaction – wherein the center-of-inertia of the aggregate follows forced convection streamlines like an aerodynamic-diameter particle an order of magnitude or so smaller than the dimension of the aggregate. The periphery of a streamline-following aggregate can ‘impact’ the boundary and add to a ‘dust’ deposition layer. Improved

discrete element method (DEM) models that include cohesive surface force models, are being developed for simulation of micron-scale pharmaceutical powders. Similar models could be applied to simulate the behavior of airborne fine particulates in crew habitat areas. The interparticle force models in the DEM codes include estimated stiffnesses for normal direction and bending-moment interactions between contacting particle-pairs. Inclusion of these cohesive forces and moments allow the simulated material to resist compaction from a relatively loose ‘floc-like’ state in a realistic manner. Uniaxial compaction tests on cohesive pharmaceutical powders, comprised of micron-scale primary particles, demonstrate the wide range of bulk-density change exhibited by powders wherein the bulk behavior is dominated by cohesive interparticle forces. DEM simulations could contribute to understanding the microstructural details of the deformation, restructuring, compaction and/or redispersion of agglomerated dust beds, in response to applied loads from the impaction of additional dust aggregates, fluctuations in air flow, or other remediation measures.

PACKED GRANULAR BEDS – Downstream from thermally cycled packed granular beds in air revitalization equipment aboard the ISS, pellet fragments and fines have been observed, which appear to have been the cause of difficulties with mechanical valves and seals in the flow system. Theoretical and experimental studies of granular solids have demonstrated that high internal stresses can be generated in packed beds, with aspect ratios greater than two, because of frictional forces transmitted to the bed walls (a form of the Janssen ‘silo’ effect). The propensity to generate high stresses in packed beds may be highly sensitive to the degree of consolidation (or void fraction remaining) and/or locked-in contact and frictional wall forces existing in the bed. Systematic variation of bed parameters such as aspect ratio, initial packing, and particle shape or size distributions in DEM simulations could provide new insight into mechanisms contributing to stress generation in packed beds. In addition, although heat conduction through pellet-pellet contacts is a small factor in overall heat transfer in systems with

interstitial gas near one atmosphere, at high vacuum, the sensitivity of contact heat transfer to the force levels existing at contacts could make pellet-pellet heat conduction a strong competitor to radiative heat transfer during heating, and thus, may increase thermomechanical stresses along already loaded 'stress trees' in the bed. The methodology for a DEM-lumped-parameter heat transfer simulation technique suitable for packed granular beds (like that proposed by McCarthy, 2003) is outlined.

APPLICABILITY OF DEM – Discrete Element Methods utilize numerical techniques nearly identical to the well known explicit particle trajectory following methods of molecular-dynamics (Allen, 1987) to calculate the motion of each individual particle in assemblies of up to 10's of thousands of interacting particles. Application of such methods for assemblies of macroscopic particles was pioneered by Cundall in the 1970's (Cundall & Strack 1979) using relatively simple engineering-mechanics-based joint-elements between contacting nearly-rigid particles. Subsequent work has demonstrated ranges of conditions under which such methods may be applicable, including collision-dominated rapid shearing granular flows and quasistatic deformation of soils and granular beds. Scale and/or mode separation allows quasistatic interparticle force relations to adequately describe even highly dynamic collisions in particulate systems as long as particle deformations are small. DEM models usually assume most particle deformation is local to the contact points, and can be approximated by linear (or non-linear) springs acting at the points of contact. Such assumptions begin to fail if stresses are so high that large plastic deformations at contacts make the contact spot-size comparable to the particle dimension, or if large elastic or plastic strains occur changing the effective shape of the modeled particles. In some cases approximate models of particle 'failure' have been incorporated (e.g., brittle fractures of individual pellets have been modeled by creation of multiple post-failure particles).

Interparticle force-displacement relations are the most important particle-scale physical properties in DEM simulations (additional key particle-scale properties include the particle shapes and the size distributions simulated). Below we describe a relatively simple (and thus, computationally straightforward) interparticle force model for DEM simulations of cohesive micron-scale particles that is physical-property based, and is expected to be robust enough to realistically simulate the mechanical behavior of low-bulk-density aggregate beds and/or low-mass-fractal-dimension aggregated clusters of particulates. A full simulation of airborne flows will need to add the gas flow and fluid-solid coupling interactions to the particle-interaction models described here. Lattice-Boltzmann approaches for the fluid flow with suspended particles (Ladd, 2001) probably would provide the most robust approach; however, other, less accurate gas-solid coupling models may be adequate for initial studies (e.g., Kawaguchi, 2000). In addition to the new model of interparticle forces for cohesive micron-

scale particles, we also describe developments that could be useful for simulations of thermomechanical stresses at another size scale, namely the millimeter-scale pellets in packed granular beds.

MICRON-SCALE INTERPARTICLE FORCES

While airborne fines in living quarters span a wide size and shape range, for simplicity, we describe here model-systems comprised of only spherical particles. Nearly cylindrical fibers will have particle-particle contacts with similar behavior, while models for flat-plate-like particles may need additional terms to account for distributed contact areas. (Arbitrary particle shapes could be simulated using artificially constructed sphere-clusters, or with other simple geometric shapes like cylindrical rods or circular plates made from annuli with planar 'lids').

PARTICULATE CLUSTER & BED BEHAVIOR – Fine particles in quiescent fluids or gases move by Brownian diffusion and randomly come in contact with other suspended particles. Simulations of cluster formation and aggregation produce aggregates with very open structures, with low mass fractal dimension. If particles 'stick' upon first contact, then cluster growth is controlled by diffusion, and the resulting Diffusion Limited Cluster Aggregation (DLCA) model aggregates have mass-fractal dimensions as low as 1.6, and may resemble the aggregate shown in Figure 1. If particles have a low probability of sticking upon contact, but touch several times before establishing a permanent cohesive contact, then a Reaction Limited Cluster Aggregation (RLCA) model simulates the growth, and produces aggregates with mass fractal dimensions around 2.6 [Bushell, 2000], consistent with experimental measurements of aggregates formed in liquid suspensions or nano-scale aerosol aggregates formed in flames [Sorensen, 1998, & 2001]. The gel points for such aggregates have solids fractions of 0.042 and 0.073 for DLCA and RLCA aggregates, respectively [Franks, 2002]. Sediment beds formed by gravity settling of aggregates start at solids fractions near the gel point, but consolidate further due to applied loads.

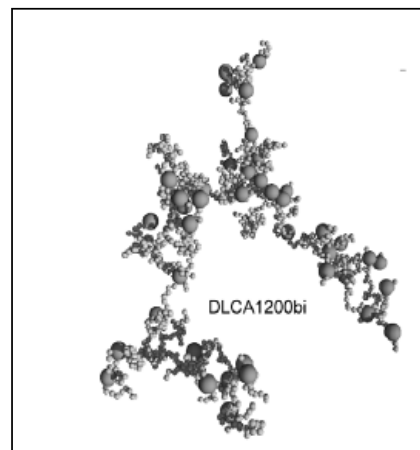


Figure 1 – Simulated DLCA aggregate comprised of 1200 spheres of two sizes [Bushell, 1998]

Simulation models for the formation of DLCA and RLCA aggregates do not allow restructuring due to bending, rotation, or breaking of contacts once they are formed. Thus, while they can assist in predicting the gel point density, they are inappropriate for use in simulating the consolidation or redispersion of sediment beds.

An example of cohesive powder bed compaction can be seen in the behavior of another model system. In a recent study of cohesive powders, a suite of chemically identical powders with various mean particle sizes was obtained by spray drying aqueous solutions of raffinose of various concentrations [Miller, 2002]. Figure 2 shows an SEM micrograph of one of those powders after storage at 33% relative humidity, allowing formation of strong bonds at some contact points.

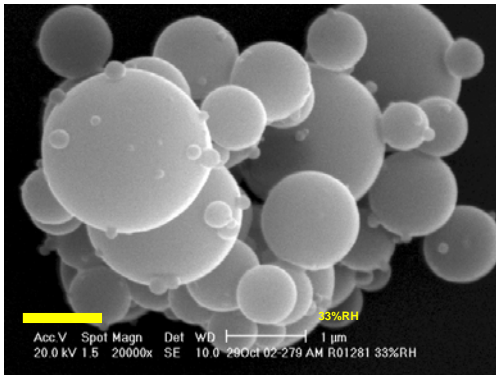


Figure 2 – Amorphous raffinose powder spray dried from aqueous solution (1 wt% solids content) in a modified Buchi spray dryer [Miller et al. 2002].

cohesive powder is around 10% to start and is only about 25% with an applied load of 10kPa (~1.5psi). This powder does not contain fibers like crew habitat dust; however, it is quite cohesive, and thus resists compaction under its own self weight, and yet, it is a very compressible bulk material. The interparticle force model described in this paper is aimed at highly cohesive powders such as this; however, similar interparticle interaction models could be applied to dust aggregates and their collected ‘sediment’ beds.

COHESIVE FORCES MODELS IN DEM

COHESION PLUS ELASTIC DEFORMATION (JKR) – All materials exhibit van der Waals forces, which arise from effective induced dipoles in the outer electron shells of the surface atoms of each particle as the surfaces approach one another. When the effects of the inverse sixth power, induced-dipole attraction of all surface atoms near the contact regions of two approaching spheres are taken into account (along with the attraction from any permanent polar orbitals), the resulting interparticle force-displacement relation takes on the form,

$$F_{vdW} = - \frac{A}{6s^2} \frac{R_1 R_2}{(R_1 + R_2)} = - \frac{AR}{12s^2} \Big|_{R_1=R_2=R}$$

where A is the Hamaker constant (*i.e.*, the combined dispersive and polar surface energy per unit area), and s is the gap spacing between the centers of the surface atoms at the point of closest approach of the two spheres, and R is the radius of a spherical particle (or radius of curvature at the point of contact for non-spherical particles). As the two particles make “contact” the outer electron shells repel each other and keep the centers of the surface atoms on the two particles about 4 \AA apart in the area where they are “touching” one another. Thus, since s never gets smaller than 4 \AA the gap spacing term, $1/s^2$, does not diverge to infinity at contact. It should be noted that the van der Waals force decreases quite rapidly as the gap between the surfaces widens. When the surface to surface spacing between two spheres is 3.6 nm , the spacing, s , between the centers of the surface atoms is 4 nm (*i.e.*, $3.6 \text{ nm} + 4 \text{ \AA}$) and the attractive force is two orders of magnitude lower than its value when they were just “touching.”

Individual particles may also carry a net charge, or even a distribution of positive and negative charges on their surfaces, which can contribute to long-range body forces between particles and with boundaries. There is a high variability in the significance of static charge on particle behavior, because the level of charge and its leak-off rate are highly dependent on environmental conditions, such as humidity, and the past history of the particles. While static electric effects should not be ignored, the high uncertainty associated with charge levels makes it a difficult phenomena to deal with. (Where charge buildup occurs in industry, remediation methods often focus on reducing sources of charge, or neutralizing charges on particles, such as by flooding a problem

Uniaxial Compaction Raffinose Powder

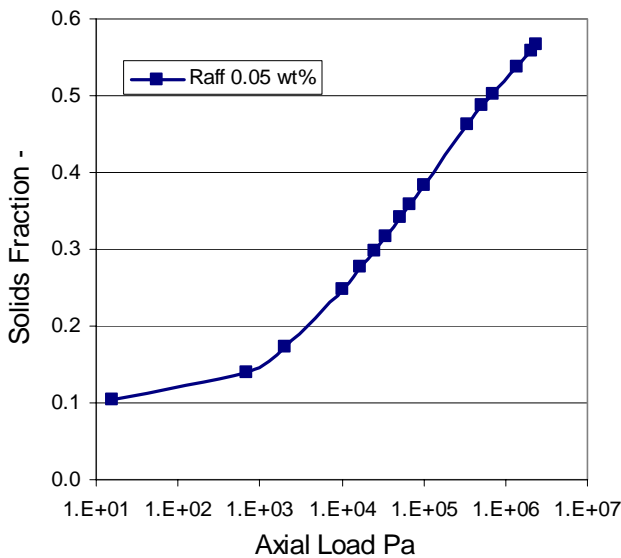


Figure 3 – Compaction of raffinose powder with volume median diameter of 0.8 microns [De Moor, 2003; Walton et al, 2003].

The compaction behavior of one of those raffinose powders, with a median size of 0.8 microns, is shown in Figure 3. Note that the solids fraction of this fine,

region with bi-polar ions). Without in any way intending to dismiss the importance of static charge effects, we will, in this paper, only deal with those forces that are part of the inherent nature of the materials, and not something that they may or may not have acquired from their environment. Thus, we will not attempt to model the effects of static charges on particles.

A reasonable starting point for a cohesive force model for dry powders is the Johnson Kendall Roberts (JKR) model which includes both linear-elastic deformation in the contact region and surface energy [Johnson, 1971]. The JKR model assumes that the interfacial forces have zero range before contact, and, in the usual application of the JKR model for cohesive contacts, the approximately $4nm$ range of those forces is, indeed, small compared to the other displacements involved. In the JKR model the total force, P , acting between two contacting bodies and the relative displacement between them, α , are given by the following equations,

$$P = \frac{4E^* a^3}{3R^*} - (8\pi\Gamma E^* a^3)^{1/2} \quad (1a)$$

$$\alpha = \frac{a^2}{R^*} - \left(\frac{2\pi\Gamma a}{E^*} \right)^{1/2} \quad (1b)$$

where, a is the contact spot radius, Γ is the surface energy per unit area, R^* is the effective radius of the contacting bodies at the contact point, and E^* is the effective modulus. R^* and E^* are given by,

$$\frac{1}{R^*} = \frac{1}{R_1} + \frac{1}{R_2} \quad (2a)$$

and

$$\frac{1}{E^*} = \frac{1-\nu_1^2}{E_1} + \frac{1-\nu_2^2}{E_2} \quad (2b)$$

where R_1 and R_2 are the radii of the contacting bodies, E is Young's modulus, and ν is the Poisson ratio.

Figure 4 shows the force-displacement relations for a non-cohesive, elastic Hertzian contact [Hertz, 1882] and the JKR model. Using this figure as a schematic we can describe salient features of the models. As particles approach, we move along the horizontal axis towards the origin from the left, with zero force for either model. As the particles touch (and α becomes positive) the non-cohesive Hertzian model gradually builds up a repulsive (positive) force that increases with the $3/2$ power of α . When contact first occurs (at $\alpha = 0$) in the JKR model, the surfaces snap together, with a net attractive force, going from the origin to point A. Then as the particles continue to approach each other, the force moves to a net zero value at point B, and then becomes repulsive (e.g. in traversing the path to point D). Upon unloading, the JKR force retraces from point D, through points B and A, and then continues (with negative α and negative force values) to points C and S, at which point the surfaces snap apart and the force returns to zero. The distance from point A to S represents outward elastic deformation of the particle surfaces as the particles are pulled apart, but before final separation occurs. The

minimum in the force-displacement relation corresponds to the pulloff force, P_c , is given by,

$$P_c = -\frac{3}{2}\pi\Gamma R^* \quad (3)$$

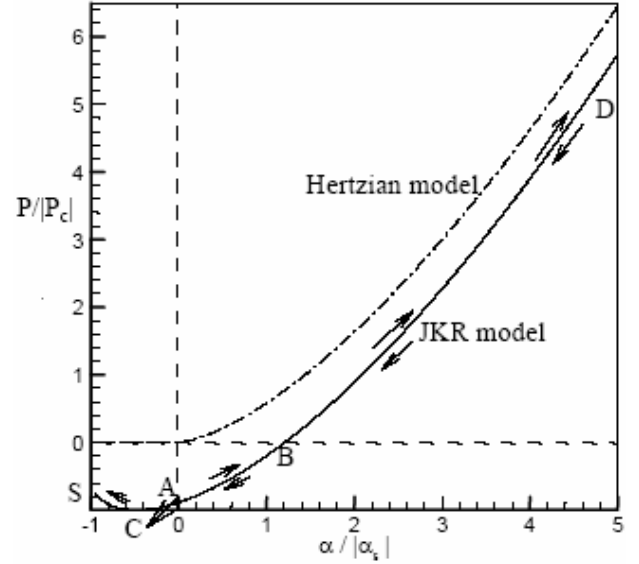


Figure 4. Force displacement relations for cohesive JKR model, and linear elastic Hertzian model [Mei, 2000].

With no applied load the particles are 'pulled' together by the cohesive force causing some deformation in the contact region. The point where the JKR curve crosses zero (point B) represents the equilibrium point with no applied loads. If applied forces pull the contacting bodies apart, they adhere to one another, deforming the surfaces outward. Final separation occurs at a displacement, α_s , given by,

$$\alpha_s = -\frac{3}{4} \left(\frac{\pi^2 \Gamma^2 R^*}{E^{*2}} \right)^{1/3} \quad (4)$$

The mathematical form of the force-displacement relation in the JKR model has been experimentally verified for macroscopic gelatin spheres [Johnson, 1985] and at the AFM (*i.e.*, nanometer) scale [Burns et al, 1999].

Shang [1998] simulated $20 \mu m$, JKR spheres with tangential sliding friction, in DEM simulations of shearing flows using both Lees-Edwards (periodic) boundaries and Couette flow (real boundaries). In the Couette flow simulations the particles formed a high density non-shearing region, held together by the cohesive forces, and a low density rapidly shearing region where the kinetic energy of collisions was high enough to break up any aggregates that formed. Solid fractions in the non-shearing regions were in the range 0.45 to 0.55. Thornton [2001] has examined the breakup of large 'clusters,' comprised of a few thousand cohesive JKR spheres, upon impact with a rigid wall. His unconfined clusters had solids fractions greater than 0.45 as well. Thus, simply adding a cohesive interparticle force to a DEM simulation model is insufficient to produce the low bulk densities exhibited by real cohesive powders.

PLASTIC DEFORMATION AT CONTACT POINTS –

The contact area predicted by Hertzian (linear-elastic) theory for contacts between smooth spheres, and for elastic JKR model spheres is usually quite small. Consequently, the total force is concentrated in such a small area that the stresses can exceed the elastic limit of the materials, even while the total force is quite low. Finite element calculations of the distribution of normal direction stress in the contact area, between perfectly elastic spheres, reproduce Hertz' theoretical hemispherical shape. If the peak normal stress exceeds $1.6Y$, where Y is the yield strength, then plastic deformation starts [Johnson, 1985]. Finite element calculations using an elastic-plastic material model show that the stress distribution flattens and covers a larger area than the Hertzian elastic model prediction. Figure 5 shows the stress distribution in the contact region between two spheres for both an elastic (Hertzian) and an elastic-plastic material model [Zhang, 2002].

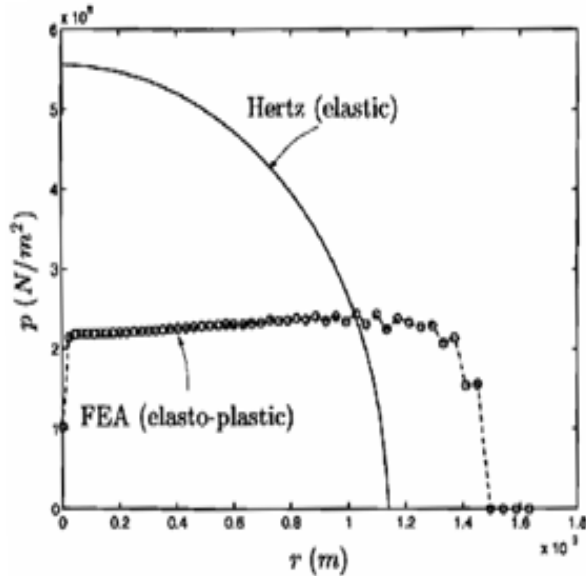


Figure 5. Normal stress distribution for contact region of elastic (Hertz) contact, and for an elasto-plastic (FEM) contact with $P \sim 40 P_Y$ [Zhang, 2002].

Careful examination of the physics involved with micron-scale particles indicates that plastic deformation is likely at contacts between particles, even if no external loads are applied. The normal force resisting the attraction between two JKR model spheres is given by the positive term in Equation (1a). With no applied load, P is zero, and the two terms on the right hand side of Eqn. (1a) cancel. At that point the repulsive force, $P_0 = 6\pi\Gamma R^*$, is four times the pull off force, P_c . This zero-applied-load repulsive force, P_0 , scales linearly with the particle size, while the load for onset of yield, P_Y , varies with the square of the particle size (Hertzian),

$$P_Y = \frac{\pi^3 R^{*2}}{6E^{*2}} (1.6)^3 Y^3 \quad (5)$$

Thus, as particle size decreases, the value of P_0 will exceed P_Y for all radii below some threshold radius, R_{0Y} . Particles smaller than R_{0Y} (or with a radius of curvature at the contact point less than R_{0Y}) will experience plastic deformation at cohesive contacts with neighboring

particles, simply due to the attractive forces (without any applied external loads). Thus, we would expect to see plastic deformations at contacts for particles smaller than 5 to $50\mu m$ in diameter (the exact threshold size depends on the values of Γ , E , and Y).

When the effects of plastic deformation, such as the flattening of the stress distribution and the widening of the contact area, are taken into account, it is observed that the plastically deformed contact region is 'flattened,' but is not truly flat. Upon unloading, the region behaves like an elastic sphere with a larger radius. As the effective radius of the 'flattened' area increases, the effective pull off force increases. Thornton and Ning developed an approximate model for such adhesive elastic-plastic contacts, with force displacement curves as shown in Figure 6.

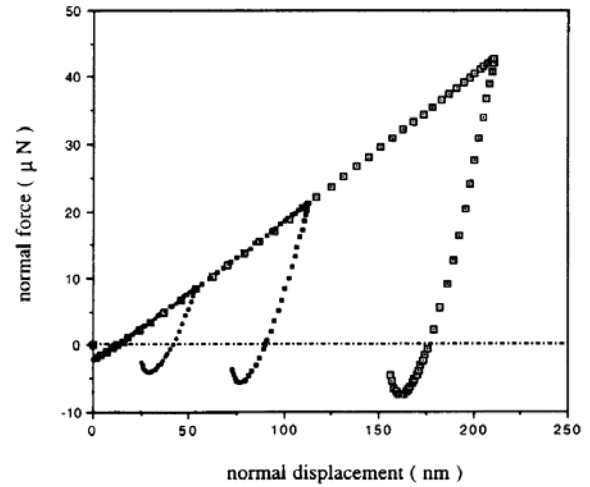


Figure 6 Force-displacement for adhesive elastic-plastic contact model [Thornton, 1998]

Like other cohesive DEM models [Thornton, 1991, 1993; Lian, 1993; Mei, 2000], Thornton's adhesive elastic-plastic [1998] model did not include any bending or twisting resistance at the interparticle contacts, and thus, allowed free rotation and rolling to occur until particles acquired multiple contacts with neighboring particles to resist such deformation modes. Simulations utilizing that model and other models have not produced the low bulk-densities exhibited by typical cohesive micron-scale powders under low loads. Instead, discrete element simulations, utilizing almost any of the currently available models for frictional and cohesive interparticle interactions, have typically exhibited solids fractions higher than 0.45, even with no applied loads, and do not produce configurations that resemble the loose structure exhibited by fine cohesive powders at low stresses.

NEW COHESION MODEL WITH BENDING MOMENTS

A new model that includes cohesion coupled with rotational resistance to bending and twisting moments about contact points is under development. The new contact model has four interrelated components

corresponding to modes of motion at the contact: *normal*, *tangential*, *bending*, and *twisting*. *Normal* refers to motion in the direction of the surface normal at the center of the contact spot, or, for spherical particles, motion parallel to a line between the centers of two contacting spheres. *Tangential* refers to relative sliding motion in the *contact plane* – a plane perpendicular to the surface normal. *Bending* refers to relative displacement of the original center of the contact spot from the line between the centers of two contacting spheres (as would occur with any rolling motion of one sphere over the surface of the other). *Twisting* refers to relative rotational motion about an axis parallel to the surface normal (or line between centers).

Various analytical models for frictional and cemented contacts have included shear and twisting resistance at contacts (e.g., Dvorkin, 1991, 1994; Mindlin, 1949, 1953; Deresiewicz, 1954); however, because bending or rolling motion was not consistent with the axial symmetry assumed in those analyses, they ignored that mode of motion. A few years ago the author of this paper developed a cemented contact model for DEM simulations of initially cemented soils and weak sandstone [Walton, 1996] that included both bending and twisting moments. In that model a linear-elastic cylinder of cement was assumed to exist at contacts, within which, failure initiated whenever strains in extreme fibers on the periphery of the cement exceeded specified failure-threshold strains. Bending and tension contributed to one failure strain threshold, while twisting and shear motions contributed to another failure threshold. The new model for cohesive powders is adapted from the author's previous cemented-contact model to conditions appropriate for micron-scale powders. In the micron-scale case, no foreign material is introduced as *cement* between contacting particles. The resistance to bending and twisting moments arises directly from the nature of surface energy related cohesive forces and the elastic and plastic deformations of the particle surfaces.

An outline of a first order form of the model proposed for interparticle contact forces and torques acting between cohesive spheres is presented below. For most of the relations we also have non-linear equations that can be implemented, if warranted; however current efforts are focused on implementing, and testing, the coupled first-order relations to see how closely they are able to mimic the compaction of the model powders.

For two spheres, *I* and *J*, let R_i and R_j be the radii, \mathbf{v}_i and \mathbf{v}_j , the translational velocity vectors, $\boldsymbol{\omega}_i$ and $\boldsymbol{\omega}_j$ the rotational velocity vectors, \mathbf{r}_i and \mathbf{r}_j the radius vectors (*i.e.*, lab frame coordinates) of the centers of the two spheres. Then the unit vector in the direction of the surface normal (*i.e.*, parallel to the line joining the sphere centers) $\hat{\mathbf{u}}_n$, is given by,

$$\hat{\mathbf{u}}_n = \frac{\mathbf{r}_j - \mathbf{r}_i}{|\mathbf{r}_j - \mathbf{r}_i|}. \quad (7)$$

The relative velocity in the *normal* direction, \mathbf{v}_n , is given by,

$$\mathbf{v}_n = [(\mathbf{v}_j - \mathbf{v}_i) \cdot \hat{\mathbf{u}}_n] \hat{\mathbf{u}}_n. \quad (8)$$

The *tangential* sliding rate, \mathbf{v}_s , is given by,

$$\mathbf{v}_s = (\mathbf{v}_j - \mathbf{v}_i) - \mathbf{v}_n + R_j(\boldsymbol{\omega}_j \times \hat{\mathbf{u}}_n) + R_i(\boldsymbol{\omega}_i \times \hat{\mathbf{u}}_n). \quad (9)$$

The *twisting* rate, $\dot{\phi}$, about the contact normal, is given by,

$$\dot{\phi} = [\boldsymbol{\omega}_j \cdot \hat{\mathbf{u}}_n - \boldsymbol{\omega}_i \cdot \hat{\mathbf{u}}_n] \hat{\mathbf{u}}_n = [(\boldsymbol{\omega}_j - \boldsymbol{\omega}_i) \cdot \hat{\mathbf{u}}_n] \hat{\mathbf{u}}_n. \quad (10)$$

The *bending* rate, $\dot{\theta}$, is given by,

$$\begin{aligned} \dot{\theta} &= \boldsymbol{\omega}_j - (\boldsymbol{\omega}_j \cdot \hat{\mathbf{u}}_n) \hat{\mathbf{u}}_n - \boldsymbol{\omega}_i + (\boldsymbol{\omega}_i \cdot \hat{\mathbf{u}}_n) \hat{\mathbf{u}}_n \\ &= (\boldsymbol{\omega}_j - \boldsymbol{\omega}_i) - [(\boldsymbol{\omega}_j - \boldsymbol{\omega}_i) \cdot \hat{\mathbf{u}}_n] \hat{\mathbf{u}}_n \end{aligned} \quad (11)$$

(The forces and moments resisting twisting and bending motions are ignored by most DEM simulation models). The incremental displacements in each direction can be obtained by integrating these relations. In finite difference form the displacement relations are,

$$\begin{aligned} \text{incremental normal displacement} & \quad \Delta \mathbf{n} = \mathbf{v}_n \Delta t \\ \text{incremental shear displacement} & \quad \Delta \mathbf{s} = \mathbf{v}_s \Delta t, \\ \text{incremental twisting displacement} & \quad \Delta \phi = \dot{\phi} \Delta t, \\ \text{incremental bending displacement} & \quad \Delta \boldsymbol{\theta} = \dot{\boldsymbol{\theta}} \Delta t, \end{aligned}$$

where Δt is the timestep. In the following model description, the magnitudes of the various force or moment components depend on the magnitudes of these displacement vectors, and the symbol, α , is used for the magnitude of the relative normal-direction displacement.

NORMAL FORCE MODEL (LINEARIZED FORM) – In the limiting case of fully plastic contacts the (repulsive) normal stress is nearly constant over a circular contact spot of radius, a , and the total (repulsive) normal force, F_R , is just the product of the stress level, σ_p , and the contact spot area, $F_R = \pi \sigma_p a^2$, where the plastic stress level is in the range $1.6Y < \sigma_p < 3Y$, which we can approximate as a constant, $\sigma_p \sim 2Y$, and the contact radius, $a \sim \sqrt{R\alpha}$, where α is the relative normal displacement. Thus,

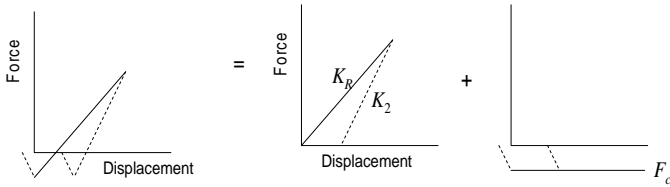
$$F_R = K_R \alpha, \quad \text{where } K_R \sim 2\pi YR.$$

Upon unloading the elastic path can be approximated as a linear unloading curve with slope, K_2 , estimated from either the initial, or average, slope of a linear-elastic, *i.e.*, Hertzian, unloading curve for a sphere with a radius that is approximately twice the original particle radius (thus, accounting for the flattening of the contact region).

A cohesive (attractive) force term is added to the repulsive normal force term to obtain the total normal force. Two forms of the cohesive force-displacement relation will be implemented; a constant attractive force (pulloff force), F_{c0} , and an attractive force level which increases linearly as the maximum compressive load experienced by the contact increases, $F_c = F_{c0} - C_f F_{Rmax}$. Here we illustrate only the constant attractive force

version. Graphically the (linearized form of the) normal force model can be represented as,

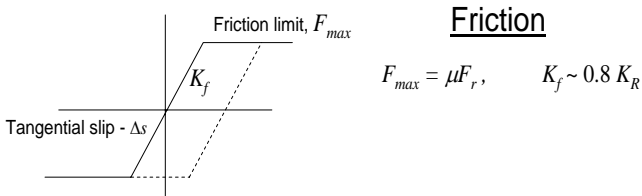
Normal Direction Force = inelastic repulsive + ~ constant cohesion



Two input quantities are required for this plastic-cohesive model, F_c , the pull-off force, and Y , the yield strength. In addition, a modified normal repulsive force stiffness, $K'_R = s_f K_R$, scaled (by an empirical factor, s_f) to account for the smaller average radii of plastically deforming asperities, may be used in place of the K_R value determined strictly from the yield strength and the particle radius.

For each of the other three displacement modes linearized forms of their force-displacement or moment-angle relations are being implemented. Later, if the simulation results indicate that important bulk behavior characteristics are sensitive to the slopes assumed in the linearized forms, then non-linear relations, such as the Mindlin-like friction model of Walton [1993b] may be added. A mathematical form that resembles an elastic-perfectly-plastic stress-strain relationship is used for each of the other modes of motion.

TANGENTIAL (ADHESIVE-FRICTION) FORCE MODEL (LINEARIZED FORM) – The tangential force, F_f , increases linearly with relative tangential sliding displacement, Δs , up to a maximum value, F_{max} , determined by the coefficient of friction, μ . The slope of the tangential force-displacement relation, K_f , will initially be assumed to be proportional to the slope of the repulsive normal force, K_R . (An alternative assumption of having the slope depend on the area of the contact spot, and thus on the value of the normal force will also be investigated). In graphical form the tangential force model is,

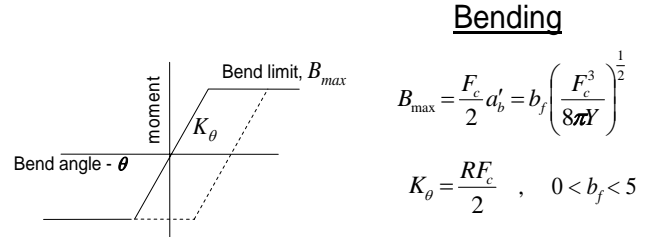


BENDING MOMENT (LINEARIZED FORM) – The assumed bending moment arises because, during a rolling motion, the contact region (or contact spot) is moving onto new surface regions of the particle. As a crescent of new surface enters the contact spot at the front, a similar sized crescent of surface leaves the contact region at the back of the rolling contact. On the front side of the rolling contact, the short range of the surface-energy based forces does not contribute to attraction until the surfaces are within a few nanometers of each other. On the back side of the rolling contact the

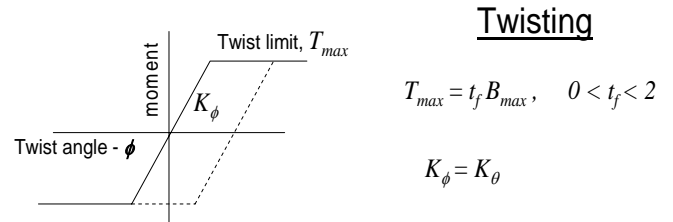
attractive forces displace the surfaces outward – holding them together longer than would be the case for undeformed spheres. This asymmetry in the contact, arising from the short range nature of the surface energy forces, and the deformations of the surfaces, results in a small moment that scales with the radius of the contact spot and with the magnitude of the attractive normal force. The radius of the contact spot will be estimated to be the size of the contact spot where the repulsive force equals the pull-off force, F_c , scaled by a factor to account for the probable condition that a real contact probably consists of several small asperities, instead of a smooth spherical surface. Distributing the normal force over several asperities reduces the assumed slope of the normal force, K_R , and also increases the effective width of the contact spot, a'_b , to

$$a'_b = b_f a = b_f \sqrt{\frac{RF_c}{K'_R}},$$

where b_f is a scaling factor (adjustable) to account for the amount of broadening occurring at the contact because of asperities. Graphically the bending moment model is,



TWISTING MOMENT (LINEARIZED FORM) – The twisting moment model is similar in form to the bending and friction models. A non-linear form, similar to that of Deresiewicz [1954], could also be implemented (and will be, if sensitivity tests show it is warranted). In graphical form the twisting moment model is,



MODEL INPUT PARAMETERS – There are a small number of physical-property-based inputs for the new interparticle interaction model, namely, F_c , the pull off force, Y , the yield strength, μ the coefficient of friction, and the amount of flattening assumed for the unloading normal force curve. In addition there are four empirical adjustment parameters that can be used to test the sensitivity of the bulk behavior of the powder assembly to the new features of the model. These adjustment parameters are:

- **Buildup** – a factor, c_r , to allow the pull off to scale with the highest normal load experienced by contact

- *Soften* – a factor, s_f , to reduce the normal stiffness to account for asperity contacts (smaller radii)



- *Widen* – a factor, b_f , to expand the contact width and moments due to asperities (for *bend* & *twist* models)
- *Twist* – a factor, t_f , by which to scale *bend* model parameters to obtain the *twist* model values

Various methods could be used to measure or estimate new model input parameters. For example, the pull off force can be obtained from AFM measurements with a functionalized tip consisting of a single particle attached to the cantilever [Quintanilla et al, 2000] (see Figure 7).

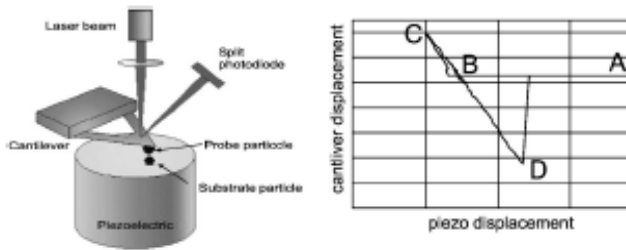


Figure 7. Experimental set-up for measurement of interparticle forces with an atomic force microscope and a typical load-unload curve [Quintanilla, 2000].

Measured values are typically a factor of 5 or so less than JKR predictions, and vary with surface roughness, indicating that surface asperities are at least as important a factor as the precise nature of the force-displacement relation assumption. Order of magnitude estimates of the pull off force could, also, be made from surface energy measurements (from inverse gas chromatography, for example). The yield strength could be estimated from literature values, or, micro-indentor AFM measurements could be used (e.g., in the literature $Y \sim 0.0035E$ for metals and $Y \sim 0.01E$ for organics, where E is Young's modulus). The coefficient of friction can be measured for macroscopic samples; however, low stress compaction results are not expected to be sensitive to its value as long as it is greater than 0.1.

The (linearized) cohesive force model, with bending moments, has a small number of input quantities based on measurable physical properties, and some additional adjustable factors that can be used to test sensitivity of simulated results to various model terms. Comparisons with measured values for compaction and/or dispersion of cohesive powder beds are planned.

THERMOMECHANICAL STRESSES IN PACKED GRANULAR BEDS

On a completely different size scale than the cohesive force discussion above (*i.e.*, millimeter instead of

micron), the behavior of packed granular beds is another potentially fruitful application area for DEM analyses, as well as some measurements on bed properties. Van der Waals cohesive forces between particles in the millimeter size range are usually completely overwhelmed by inertial, aerodynamic and/or even electrostatic forces. Thus, no cohesive interaction force model is usually needed for simulations of packed beds of millimeter-scale pellets. Improved boundary conditions, thermal expansion models, and new discrete (lumped parameter) heat transfer calculations could allow DEM models to provide useful insights on the thermomechanical stresses developed in thermally-cycled packed beds.

STRESSES IN PACKED BEDS – The potential effect of wall friction on stresses in packed granular beds is a phenomena that is often overlooked or poorly understood. It can lead to extremely high stresses in the material, or can, as in the case of silos that Janssen [1895] analyzed, lead to much lower stresses than might be anticipated. Janssen utilized a differential-slice analysis to evaluate the horizontal and vertical stresses in granular materials inside storage silos and explained why most of the vertical load is transferred to the silo walls. A similar analysis can be used to show why the force required for a piston to move a granular material up a vertical pipe increases exponentially with the height of the granular bed being pushed.

Referring to Figure 8 and following the logic of Janssen we consider two cases: 1) gravity acting down with wall friction acting up, resisting the downward movement of the material (*i.e.*, Janssen's case); 2) a piston pushing the slug up from the bottom with gravity acting down, and wall friction acting down. The granular material is assumed to be in a vertical cylindrical container of radius, R , with a wall friction coefficient, μ (for friction between the granular material and the pipe wall). A few simplifying assumptions are made:

- The vertical stress is constant over a planar horizontal cross-section.
- The ratio between the horizontal and the vertical stress within the slice is a constant, $k = \sigma_h / \sigma_y$.
- The wall friction is 'fully developed' so that the vertical stress at the wall $\sigma_f = \mu \sigma_h$, and acts in a direction to resist relative motion between the pipe wall and the granular material.
- The bulk density, ρ , of the granular material is essentially constant throughout the bed.

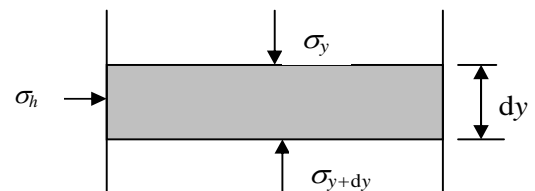


Figure 8 – Differential slice for force balance analysis.

A vertical force balance analysis on the differential slice produces a first order, ordinary differential

equation for the vertical stress in the granular material (y is assumed to be zero at the top surface and increases with depth).

Force down = Force up

$$\rho g \pi R^2 dy + \sigma_y \pi R^2 = 2 \pi R \mu \sigma_h dy + \pi R^2 \sigma_{y+dy}$$

rearranging and simplifying:

$$\frac{\sigma_{y+dy} - \sigma_y}{dy} + \frac{2\mu\sigma_h}{R} - \rho g = 0$$

or, noting that $\sigma_h = k\sigma_y$, we obtain,

$$\frac{d\sigma_y}{dy} + \frac{2\mu k}{R} \sigma_y - \rho g = 0 \quad (12)$$

Janssen's solution to this ODE is obtained if we assume that the stress, σ_y , is zero at the top free surface (where $y = 0$). The resulting vertical stress distribution solving Eqn (12) is,

$$\sigma_y = \frac{\rho g R}{2\mu k} \left(1 - e^{-\frac{2\mu k}{R} y} \right) \quad (13)$$

where g = the acceleration of gravity. This is the well known Janssen formula for vertical stress in the material stored in a silo. Note that as y increases the exponential term vanishes, so that the maximum value of the vertical stress in the material, $\sigma_{y \max} = \frac{\rho g R}{2\mu k}$, scales with the

radius of the silo, in contrast to pressure in a liquid which would scale linearly with the depth, and be independent of container radius.

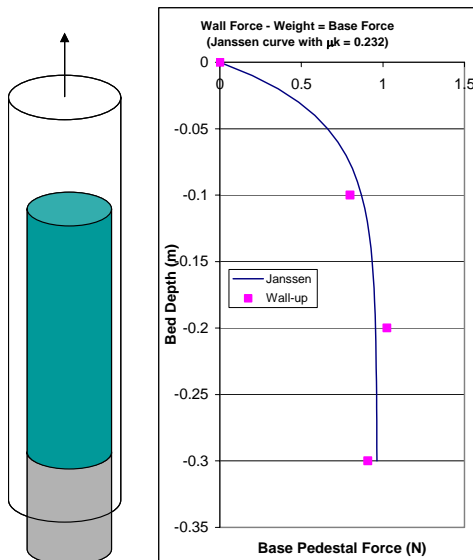


Figure 9. Force on base pedestal as wall is pulled up as a function of bed height. Symbols – 3mm glass beads in 4cm acrylic pipe, Line – Equation (13), [Walton, 1999].

Equation (13) has been verified for static granular beds in silos many times during the past 100 years. Students at the University of Florida verified it by placing various depths of 3mm glass beads in a 4cm diameter acrylic pipe with a slightly smaller diameter cylindrical pedestal

forming the base of the glass-bead bed. The pipe was pulled up in an Instron universal test apparatus and the force required to move the pipe recorded as a function of the bed height. This setup replicates the assumptions of Janssen's silo analysis and the force on the bottom pedestal approached the Janssen asymptotic value when the bed height was a few pipe diameters. The coefficient of friction and the ratio of axial to radial stress were not measured in these tests, so that the product μk became a fitting parameter for the Janssen prediction of vertical force. Figure 9 shows the Janssen theory, Eqn (13), and the measured vertical load at the base.

If we consider the case where the material is being pushed up (as, for instance, by a piston) from the bottom, then friction acts in the opposite direction – resisting the upward motion. The differential slice analysis and force balance can be repeated under these conditions,

Force down = Force up

$$\rho g \pi R^2 dy + \sigma_y \pi R^2 + 2 \pi R \mu \sigma_h dy = \pi R^2 \sigma_{y+dy}$$

rearranging and simplifying as before:

$$\frac{d\sigma_y}{dy} - \frac{2\mu k}{R} \sigma_y - \rho g = 0 \quad (14)$$

again assuming $\sigma_y = 0$ at the top we obtain the solution for the vertical stress as a function of the bed height,

$$\sigma_y = \frac{\rho g R}{2\mu k} \left(e^{\frac{2\mu k}{R} y} - 1 \right) \quad (16)$$

This time the exponent is positive, so we find stress increasing exponentially with the bed length being pushed up. This result has been verified experimentally as well [Walton, 1999; Arroyo-Cetto, 2003]. When the 4cm acrylic pipe wall containing beds of 3mm glass beads of various heights (described previously) was pushed down, the stationary pedestal acted as a piston pushing the beads up. Figure 10 repeats the results of Fig 9 (wall up) and also shows force measurements when the pipe was moving down; except here the graph is semi-log with the force on the vertical (log) axis.

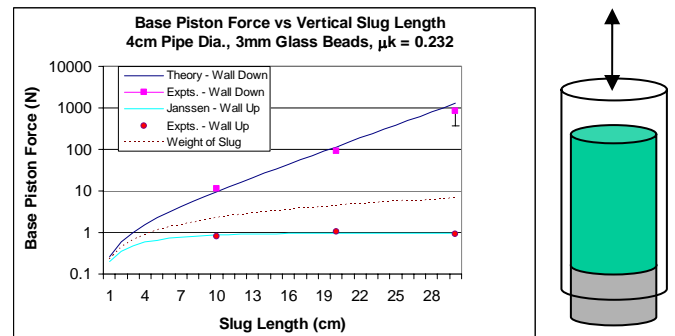


Figure 10 – Repeat of Fig (9) test plus pipe wall moving down data verifying the exponential form of Eqn (16). The same $\mu k = 0.232$ value was used for both curves [Walton, 1999].

The value of $\mu k = 0.232$ from the Janssen (wall up) test, was used in Eqn 16 to obtain the wall-down line shown

in Fig 10. The experimental results verify the exponential form of the force vs. bed height relationship of Eqn (16). This also explains why it is nearly impossible to push a very long slug of granular material through a pipe unless something fails (e.g., either the pipe wall or the granular material).

The relevance of these results to packed beds used for air revitalization, such as the Carbon Dioxide Removal Apparatus (CDRA) aboard the ISS, can be illustrated by considering an experiment described in Zenz & Othmer's [1960] text on fluidized beds. In the test described by Zenz, a granular material is exposed to a condition (e.g. water) that causes it to expand. That condition propagates slowly through the column causing the affected material behind the propagation front to expand (see Figure 11). The packed granular beds aboard the ISS undergo thermal cycling for regeneration, and during such cycles the material will experience some thermal expansion. The designs allow room for this expansion via movable lids that are spring loaded to maintain a low level of axial stress on the end of the bed (e.g. see Figure 14). Although not a thermal expansion test, the experiment in Fig 11 demonstrates the effects observed when a packed bed of granular material expands gradually from one end, inside a vertical pipe. Similar behavior would be expected if the material were heated from the top end (and the container had a lower thermal expansion coefficient than the granular bed material). For this test, and the previously described piston pushing glass beads up a pipe, the initial stresses due to the gravitational field are very small compared to the loads eventually applied by the piston or by the 'swelling' material. All that is necessary for the high stresses to develop is that sufficient axial stress exists, initially, so that additional axial loads will cause an increase in the radial stress. In the packed beds on the ISS the spring-loaded lids provide an initial axial load sufficient to ensure that stresses perpendicular to the axis will develop in the bed, and that wall friction can contribute to the overall stress state in the granular bed.

The examples above illustrate some of the general trends observed in packed granular beds, however, a more complete characterization of granular bed properties would show that the material property assumptions in a Janssen-like theoretical analysis are not exactly followed, even by assemblies of mono-disperse spheres. For the same 3-mm glass beads described in tests of Figs (9) and (10), a short (3-cm tall) bed of beads was compressed between two pistons at various fixed loads, and the force required to move the surrounding pipe wall up and down measured. Figure 12 shows that while the value of $\mu\sigma_r$ varied linearly with axial stress, σ_z , the line did not pass through the origin as would be the case if the material obeyed the assumptions of the analysis above. The reason for the apparent 'cohesive-like' behavior is due to shear-dilatant forces which are a strong function of the packing fraction of the bed. Uniform sized spheres can be packed as dense as an fcc lattice with a solids fraction of 0.74 or as

loose as a cubic lattice with a solids fraction of 0.524; however, a typical bed of spheres placed in a container, and tapped or vibrated to densify the bed, will arrive at random close packing with a solids fraction of about 0.63. In order to avoid shear dilatant effects upon deformation, a bed of uniform size spheres would need to be at or near the random loose packing limit of 0.58. We would expect glass beads initially consolidated to a different packing fractions to produce lines with slopes similar to that shown in Figure 12, but with intercepts that could be near zero (Janssen's assumption) or as much as an order of magnitude higher.

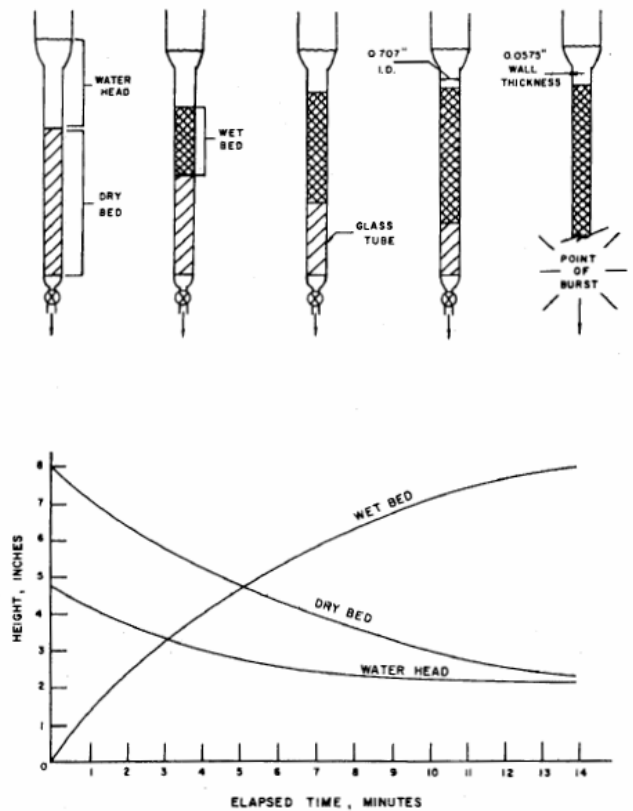


Figure 11 – "... illustrates the progress of an experiment in which water is poured on a bed of dry organic copolymer ion-exchange resin and allowed to permeate by gravity downward through the bed. After 14 min, when the water had trickled down through a wet-bed depth of 8 in, the glass column burst. The dry solids below the interface between the wet resin and the dry resin constituted an effective piston, since they were so confined that they could not expand downward. The upward force pushing against the wet bed was developed by wetting the dry resin particles at the interface and their consequent swelling. At the moment of rupture, the wet-bed depth had exceeded the longest movable core of these resin particles in the 0.707 in-diameter tube. . . ." [Zenz, 1960, (p78-79)]

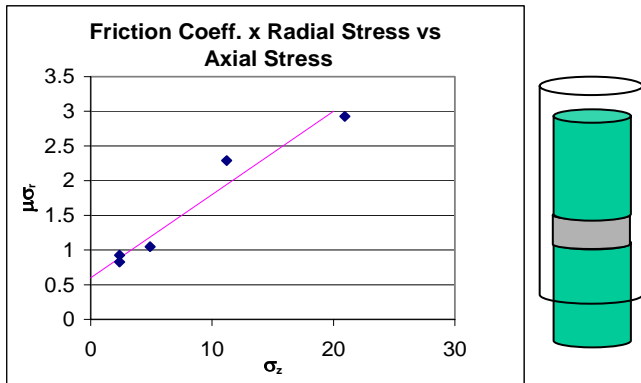


Figure 12 – Variation of radial stress (times the friction coefficient) with axial stress in packed bead bed.

Without cohesive forces, discrete element model (DEM) simulations of sphere packing is significantly denser than the low solids fractions observed for fine cohesive powders. Figure 13 shows the results of DEM simulations of sphere-packing obtained by dropping smooth (*i.e.*, frictionless) and frictional spheres into a rectangular region between two fixed vertical planes, spaced ten particle diameters apart. The average solids fraction for the monodisperse smooth spheres is 0.63 – very nearly equal to *random close packing* for uniform spheres. The solids fraction for the frictional spheres is approximately 0.57. The graphs of the solids fraction distributions across the widths of the cells, show that there are significant ‘wall effects’ which extends several particle diameters into the sphere assemblies.

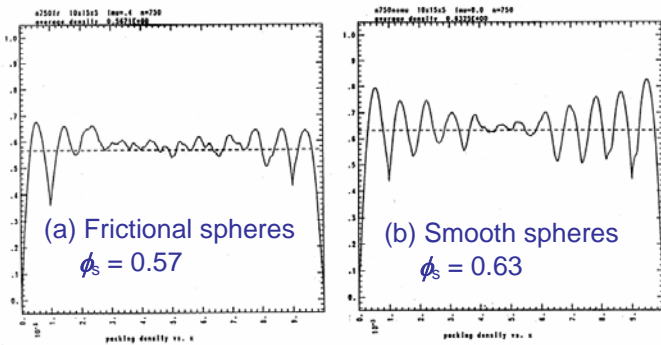
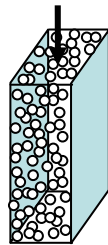


Figure 13 – Average solids fraction as a function of distance from the wall for (a) frictional and (b) frictionless spheres with a gap width of 10 sphere diameters [Walton, 1993a].

The frictional-sphere case of Fig 13 is not unlike a typical granular bed which is filled by pouring pellets into a container under terrestrial conditions. In the simulation, the packing ended up quite near the random-loose-packing limit for uniform size spheres. At this

packing density the material is likely to behave like a normally-consolidated, or slightly under-consolidated, soil (*i.e.*, it could shear at constant volume without producing high normal stresses). The simulation of frictionless spheres, on the other hand, provides an indication of what density might be obtained if a bed of frictional spheres is subjected to vibration (momentarily lowering normal forces at contacts, and thus, effectively reducing contact friction forces) while in a gravitational field, or with a compressive load applied. Any shear deformation of a bed of spheres at this packing is likely to produce very high normal stresses due to shear-dilatant effects, typical of over-consolidated soils. Recent tests of pistons pushing bead-beds have shown that the forces can be as much as a factor of five higher when the packing fraction of the bead-bed is increased by as little as 3.5% [Arroyo-Cetto, et al., 2003]. Campbell has reported stress level increases in dense sheared granular flows of up to three orders of magnitude resulting from an increase in solids fraction of approximately 2% [Campbell, 2002].

The original designs of four packed pellet beds in the Carbon Dioxide Removal Apparatus (CDRA) aboard the ISS included spring-loaded lids intended to keep the pellets under a small confining load (and thus, prevent open channels from forming during gas flows under microgravity), (see Figure 14).



Figure 14 – Examples of ISS – CDRA packed granular beds and a spring-loaded ‘floating-lid’.

Problems eventually developed from pellet related fines in mechanical equipment (valves and seals) downstream from some of the beds. Upon inspection (Jan 2003) after return to earth (Oct 2002) it was observed that larger-than-expected movements of the ‘floating’ plate lids had occurred in these beds. One hypothesis for the large movement of the lids is that they occurred during the vibrations of the launch environment. The lid displacements were sufficient to change the bulk packing fraction of the pellets in some of the beds by several percent. Such changes in bed-packing can have a dramatic effect on stress generation in response to any bed deformation as described above. Thermo-mechanical stresses might be significantly higher in a packed bed which has been vibrationally densified by a

few percent after initial filling, than they would have been if the bed had not experienced the increase in packing.

The above hypotheses and other effects in thermally cycled packed beds could be explored computationally via DEM simulations. Stresses in packed beds with aspect ratios exceeding two, and subject to thermal expansion of the constituent bed particles, could be simulated with relatively straightforward modifications to currently existing DEM models. If non-spherical particles (such as typical packed bed pellets) were to be simulated, then more extensive enhancements would be needed. Sphere clusters have been simulated by a number of researchers (e.g., Walton & Braun, 1993). A relatively small number of DEM codes have utilized more complex shapes (e.g., Hopkins, 1999); however, the numerical methods exist – only the implementation details are burdensome.

Heat transfer in packed beds is usually dominated by conduction in the interstitial gas. The small effective area of contact between particles makes particle-particle heat transfer by conduction quite small. At high vacuum, the usual assumption is that most heat transfer is via radiative transfer. However, since particle-particle conduction is a strong function of the contact area, and the contact area depends strongly on the normal stress at the contact point, it is possible that thermally cycled granular beds in high vacuum will have a significant particle-particle conductivity contribution to total heat transfer. This hypothesis could be tested experimentally quite easily. Also, if particle-particle conduction is contributing a significant role in the packed bed heat transfer, then an enhanced DEM heat transfer technique, based on a lumped-parameter model with a stress-level-dependent 'heat conduction' through contact points (McCarthy, 2003), could be used to study the range of non-uniformities in temperature that might develop (because 'stress trees' in the bed might become high conductivity pathways).

CONCLUSION

For micron-scale particulate systems the inclusion of cohesion, along with realistic moment resistances at interparticle contacts, will allow discrete-particle models to simulate the particle-scale restructuring that occurs when external loads and body forces are applied to loosely aggregated beds of cohesive powder particles. At the extreme of infinite resistance to bending, one would expect simulated aggregates to resemble those from cluster aggregation simulation models, which do not allow any restructuring once a contact is made. It is expected that the cohesive force model described in this paper will be able to simulate aggregates with structures somewhat like that shown in Figure 1, except that the new model will allow such an aggregate to restructure (by rotating, twisting, or breaking of contacts) in response to applied loads or body forces. Simulations of the detailed particle-scale rearrangements could provide insight into understanding, as well as adding the ability

to predict, both the compaction and redispersive behavior of cohesive powders.

On a millimeter scale DEM simulations might provide useful new insight into thermomechanical stresses in thermally cycled packed granular beds (especially if a lumped-parameter contact-load-dependent particle-particle conduction model is implemented).

ACKNOWLEDGMENTS

All measurements of the model raffinose powders were conducted by Nektar Therapeutics, San Carlos, CA. They have provided encouragement and assistance in this work, which is gratefully acknowledged. Measurements of glass beads were performed at the NSF Engineering Research Center for Particle Science and Technology at the University of Florida in 1998, during the time the author was a faculty member at UF and received support from the Center.

REFERENCES

- Allen, M.P., and D.J. Tildesley, *Computer Simulation of Liquids*, Clarendon Press, Oxford (1987).
- Arroyo-Cetto, D., G. Pulos, R. Zenit, M.A. Jimenez-Zapata, and C.R. Wassgren, "Compaction force in a confined granular column," *Phys. Rev. E*, **68**, 051301 (2003).
- Burns, A.R., J.E. Houston, R.W. Carpick, and T.A. Michalske, "Friction and Molecular Deformation in the Tensile Regime," *Phys. Rev. Lett.*, **82**, 6, p1181 (1999).
- Bushell, G.C. (1998) *Primary Particle Polydispersity in Fractal Aggregates*, PhD dissertation, University of New South Wales
- Bushell, G.C., Y.D. Yan, D. Woodfield, J. Raper and R. Amal, "On techniques for the measurement of the mass fractal dimension of aggregates", *Advances in Colloid and Interface Science*, **95**, 1-50, (2000).
- Campbell, C.S., *J. Fluid Mech.* **465**, 261 (2002).
- Cundall, P.A., and O.D.L. Strack, "A Discrete Numerical Model for Granular Assemblies," *Geotechnique*, **29**, 47-65 (1979).
- De Moor, C.P., (2003) Nektar Therapeutics, San Carlos, CA (Private Communication)
- Deresiewicz, H. (1954) "Contact of elastic spheres under an oscillating torsional couple," *Trans. ASME, Journal of Applied Mechanics*, **21**, 52.
- Dvorkin, J., Mavko, G., and Nur, A., 1991, "The Effect of Cementation on the Elastic Properties of Granular Material", *Mechanics of Materials*, **12**.
- Dvorkin, J., Nur, A., and Yin, H., 1994, "Effective Properties of Cemented Granular Materials", *Mechanics of Materials*, **18**.
- Franks, G.V., S. Weseloh, I.D.P. Westra, Y.D. Yan, G.J. Jameson and S. Biggs (2002) "Controlling size and structure of particle aggregates by solids concentration

and shear”, Proceedings of World Congress on Particle Technology 4, Sydney, Australia, July 21-25, 2002.

Hanes, D., and O.R. Walton (2000) “Simulations and physical measurements of glass spheres flowing down a bumpy incline,” *Powder Technology*, **109**, pp133-144.

Hertz, H. (1882) Über die Berührung fester elastische Körper (On the contact of elastic solids), *J. reine und angewandte Mathematik*, **92**, 156-171. (for English translation see *Miscellaneous Papers by H.Hertz*, Eds. Jones and Schott, London, Macmillan, 1896).

Hopkins, M.A., & J Tuhkuri “Compression of floating ice fields,” *J. Geophys. Res.*, **104**(C7) 15815-15825 (1999).

Janssen, H.A., “Versuche über Getreidedruck in Sillozen,” *Zeit. Ver. Duetsch. Ing.*, **39**, 1045-1049 (1895).

Johnson, K.L., K. Kendall, and A.D. Roberts (1971) “Surface energy and the contact of elastic solids,” *Proceedings, Royal Society*, **A324**, 301

Johnson, K.L. (1985) *Contact Mechanics*, Cambridge Univ. Press, London.

Kawaguchi, T., M. Sakamoto, T. Tanaka, & Y. Tsuji “Quasi-three-dimensional numerical simulation of spouted beds in cylinder,” *Powder Technology*, **109**, 1-3, p3-12 (2000).

Ladd, A.J.C., and R. Verberg, “Lattice-Boltzmann Simulations of Particle-Fluid Suspensions,” *J Stat. Phys.* **104**, 516, p1191 (2001).

Lian, G., C. Thornton, M.J. Adams (1993) “Effect of liquid bridge forces on agglomerate collisions,” *Powders & Grains*, Thornton, ed., Balkema, Rotterdam, 59-64.

McCarthy, J., “Discrete Modeling of Heat Transfer in Particulate Systems,” *AIChE Annual Mtg* (2003) ppr 43g

Mei, R., H. Shang, O.R. Walton, J.F. Klausner (2000) “Concentration non-uniformity in simple shear flow of cohesive powders,” *Powder Technol.*, **112**(1-2), 102-110.

Mindlin, R.D., *J. Appl. Mech. (Trans. ASME)* **16**, 259 (1949)

Mindlin, R.D., and H. Deresiewicz, *J. Appl. Mech (Trans. ASME)* **20**, 327 (1953).

Miller, D. P., D.Lechuga-Ballesteros, L. Williams, T. Tan, J. Kanda, W. Foss, O. Walton, A. Mandel, and X. Cai (2002) “Dispersibility of Spray-dried Raffinose: Effects of Particle Size and Relative Humidity,” *AAPS Annual Meeting and Exposition - November 10-14, 2002 - Toronto, Canada*.

Quintanilla, M. , A. Castellanos, & J. M. Valverde, (2000) “Correlation between bulk stresses and inter-particle contact forces in fine powders”, *Phys Rev E*, **64**, 031301.

Shang, Hong, (1998) “Simulation and modeling of cohesive powder flow”, Ph.D dissertation, University of Florida, Gainesville, FL.

Sorensen, C.M., W.B. Hagemann, T.J. Rush, H. Huang, and C. Oh, (1998) “Aerogelation in a Flame Soot Aerosol,” *Phys. Rev. Lett.* **80**, 1782.

Sorensen, C.M. (2001) “Light Scattering from Fractal Aggregates. A Review,” *Aerosol Sci. Tech.*, **35**, 648.

Thornton, C. and Yin, K.K. (1991) “Impact of Elastic Spheres With and Without Adhesion,” *Powder Technology*, **65**, 153-166

Thornton, C., Lian, G. and Adams, M.J. (1993) “Modeling of Liquid Bridges Between Particles in DEM Simulations of Particulate Systems,” *Proc. of 2nd Int'l. Conf. on Discrete Element Methods (DEM)*, J.R. Williams and G.W. Mustoe, eds., IESL Pub., MIT, Cambridge, MA.

Thornton, C. and Z. Ning, (1998) “A theoretical model for the stick/bounce behaviour of adhesive elastic-plastic spheres,” *Powder Technology*, **99**, 154-162.

Thornton, C., in *Proc. AIChE Annual Mtg., Particle Technology Forum*, Los Angeles, November (2001)

Walton, O.R. (1993a) “Simulation of Gravity Flow and Packing of Spheres,” in *Proc. Nisshin Engineering Particle Technology International Seminar (NEPTIS-1)*, Jan 18-20, Osaka, Japan.

Walton, O.R., “Numerical simulation of inclined chute flows of monodisperse, inelastic, frictional spheres,” *Mechanics of Materials*, **16** (1993b) 239-247.

Walton, O.R. & R.L. Braun (1993) “Simulation of Rotary-Drum and Repose Tests for Frictional Spheres and Rigid Sphere Clusters,” *Joint DOE/NSF Workshop on Flow of Particulates and Fluids* Sep 29 – Oct 1, 1993, Ithaca, NY.

Walton, O.R. (1996) [personal communication] *Cemented Contact Model Algorithms for Assemblies of Spherical Particles*, Grainflow Dynamics Report to Caterpillar, Livermore, CA, Sept. 10, 1996 (Final Report, Contract 340.914C)

Walton, O.R., R. Mei, D. Hanes “Quasistatic Micro-Scale to Macro-Scale Connection,” in *University of Florida ERC Annual Report to NSF*, B. Moudgil, ed. (1999)

Walton, O.R., C.P. De Moor, D.P. Miller (2003), “Simulation of Low-Stress Compaction of Cohesive Micron-Scale Powders,” *AIChE 2003 Annual Meeting*, San Francisco, CA, November 16-21 (Session T4-35a).

Zhang, X. ,and L. Vu-Quoc (2002) “Modeling the dependence of the coefficient of restitution on the impact velocity in elasto-plastic collisions,” *Int'l. J. Impact Eng.* **27**, 317-341.

Zenz, F.A., and D.F. Othmer, *Fluidization and Fluid Particle Systems*, Reinhold Publishing, 1960

CONTACT

walton@grainflow.com

Grainflow Dynamics

PMB #270, 1141 Catalina Drive, Livermore, CA 94550

